Molecular Biology of the Cell
Vol. 17, 3557–3568, August 2006

Infection with Replication-deficient Adenovirus Induces Changes in the Dynamic Instability of Host Cell Microtubules[D]

James C. Warren, Adam Rutkowski, and Lynne Cassimeris

Department of Biological Sciences, Lehigh University, Bethlehem, PA 18015

Submitted September 11, 2005; Revised May 24, 2006; Accepted June 1, 2006
Monitoring Editor: J. Richard McIntosh

Adenovirus translocation to the nucleus occurs through a well characterized minus end-directed transport along microtubules. Here, we show that the adenovirus infection process has a significant impact on the stability and dynamic behavior of host cell microtubules. Adenovirus-infected cells had elevated levels of acetylated and detyrosinated microtubules compared with uninfected cells. The accumulation of modified microtubules within adenovirus-infected cells required active RhoA. Adenovirus-induced changes in microtubule dynamics were characterized at the centrosome and at the cell periphery in living cells. Adenovirus infection resulted in a transient enhancement of centrosomal microtubule nucleation frequency. At the periphery of adenovirus-infected cells, the dynamic instability of microtubules plus ends shifted toward net growth, compared with the nearly balanced growth and shortening observed in uninfected cells. In infected cells, microtubules spent more time in growth, less time in shortening, and underwent catastrophes less frequently compared with those in uninfected cells. Drug-induced inhibition of Rac1 prevented most of these virus-induced shifts in microtubule dynamic instability. These results demonstrate that adenovirus infection induces a significant stabilizing effect on host cell microtubule dynamics, which involve, but are not limited to, the activation of the RhoGTPases RhoA and Rac1.

INTRODUCTION

Adenoviruses (Ad) are nonenveloped double-stranded DNA viruses that enter the host cell by receptor-mediated endocytosis and use dynein motor proteins to traverse the cell on microtubules (MTs). The MT minus end-directed motility quickly directs Ad within proximity to the nucleus, where viral replication occurs (Kelkar *et al*., 2004; Meier and Greber, 2004). Ad infection is initiated by a two-step binding process in which the Ad fiber knob binds the host cell coxsackie-adenovirus receptor (Bergelson *et al*., 1997), whereas the RGD-motif of the Ad penton base binds cellular $\alpha_v\beta_5/\beta_3/\beta_1$ integrins (Wickham *et al*., 1993; Nemerow and Stewart, 1999). The internalization of Ad coincides with a number of integrin-dependent signal cascades, including the activation of focal adhesion kinase (FAK) and phosphoinositide 3-kinase (PI3K) (Greber, 2002). A major consequence of Ad-induced signaling is the substantial rearrangement of the host cell actin network, including the formation of lamellipodia and filopodia, which is mediated by the small Rho-family GTPases Rac and CDC42 (Li *et al*., 1998a).

This article was published online ahead of print in *MBC in Press* (http://www.molbiolcell.org/cgi/doi/10.1091/mbc.E05–09–0850) on June 14, 2006.

[D] The online version of this article contains supplemental material at *MBC Online* (http://www.molbiolcell.org).

Address correspondence to: James Warren (jaw8@lehigh.edu).

Abbreviations used: Ad, adenovirus; Ad-AF555, adenovirus conjugated to Alexa Fluor 555; ASFV, African swine fever virus; FAK, focal adhesion kinase; HHV, human herpesvirus; HSV, herpes simplex virus; k_c, catastrophe frequency; k_r, rescue frequency; MT, microtubule; PI3K, phosphoinositide 3-kinase.

In addition to their well-characterized regulation of the actin cytoskeleton, the RhoGTPase family regulates MT dynamics (Rodriguez *et al*., 2003). MTs undergo a nonequilibrium process of growth and shortening known as dynamic instability (Desai and Mitchison, 1997), and modulation of these dynamics occur frequently in interphase cells. In migrating cells, Rac1 regulates the dynamics of MTs to favor formation of stable "pioneer" MTs. These pioneer MTs are biased toward net growth and extend into the lamellipodia (Wittmann *et al*., 2003). At fibroblast cell wound edges, RhoA regulates the formation of stable MTs in a process that is dependent upon the integrin-mediated activation of FAK (Palazzo *et al*., 2004).

MT dynamic turnover is likely to influence the rate of viral trafficking to the nucleus. Paclitaxel-induced suppression of MT dynamics enhanced Ad nuclear localization (Giannakakou *et al*., 2002), suggesting that the dynamic state of MTs could contribute to Ad transport. In addition, Ad binding to cellular integrins activates signals that enhance the MT-mediated nuclear localization of internalized virions (Suomalainen *et al*., 2001). These observations suggest that Ad infection and subsequent signaling may modulate the MT dynamics of the host cell, generating stable MTs to support the intracellular transport of the virus.

Virus-induced modulation of MT dynamics has been previously identified by measuring levels of MT acetylation, one of several tubulin modifications associated with stable, nondynamic MTs (Piperno *et al*., 1987). Several viruses, including herpes simplex virus (HSV) type 1, African swine fever virus (ASFV), and reovirus, induce MT acetylation within 9–18 h after infection (Parker *et al*., 2002; Jouvenet *et al*., 2004; Yedowitz *et al*., 2005). In contrast, human herpesvirus (HHV) type 8 induced the acetylation of host cell MTs as early as 30 min postinfection in a process that required the

binding of virus to cellular integrins and active RhoA (Naranatt *et al*., 2005). The RhoA-mediated stabilization of MTs in HHV-8–infected cells has been proposed to be essential for nuclear-directed virus transport (Krishnan *et al*., 2006).

In the current study, we have analyzed both the stable and the dynamic populations of cellular MTs after infection of the host cell with a replication-defective Ad. Consistent with studies of other viruses, we found that Ad infection enhances the levels of stable, posttranslationally modified MTs. MT acetylation and detyrosination occur within 1–2 h postinfection and are dependent upon active RhoA. We also found that Ad infection induces Rac1-dependent changes in the dynamic population of MTs, characterized by increased time spent in growth, decreased frequency of catastrophes, and a shift in the balance of MT dynamic instability toward net growth. These data provide the first description of virus-induced modulation of the dynamic subset of MTs.

MATERIALS AND METHODS

Cell Culture

Human lung carcinoma cells (A549; ATCC CCL-185) were maintained at 37°C in a humidified incubator set at 5% CO_2, grown in F-12 (Invitrogen, Carlsbad, CA) medium supplemented with 10% fetal bovine serum (FBS) (Invitrogen), 1.5 g/l sodium bicarbonate (Sigma-Aldrich, St. Louis, MO), and 1× antibiotic/antimycotic (Sigma-Aldrich). Human foreskin fibroblast (HFF) cells (HFF-1; ATCC SCRC-1041) were grown in DMEM (Invitrogen) supplemented with 10% FBS, 1.5 g/l sodium bicarbonate, and 1× antibiotic/antimycotic. For experiments using serum starvation, HFF cells were grown for a total of 2 d in serum-free DMEM supplemented with 1 mg/ml fatty acid-depleted bovine serum albumin. Human embryonic kidney 293 cells (ATCC CRL 1573) were grown in minimal essential medium (Invitrogen) supplemented with 10% FBS, 1.5 g/l sodium bicarbonate, and 1× antibiotic/antimycotic. All cell lines were subcultured twice per week as per American Type Culture Collection (Manassas, VA) recommendations. HFF cells were maintained for up to 7 wk, or ~40 doublings, after which the culture was discontinued.

Transfections

The EB1-green fluorescent protein (GFP) plasmid was described previously (Piehl and Cassimeris, 2003). The α-tubulin-GFP plasmid was obtained from Clontech (Palo Alto, CA). Transfections were typically performed 1 d after seeding cells on round 30-mm coverslips, when cells were typically at 20–40% confluence. Cells were transfected using FuGENE transfection reagent (Roche Applied Science, Indianapolis, IN) according to the manufacturer's recommended protocol. Imaging of transfected cells was performed on the second day posttransfection. Overexpression of the GFP-tubulin fusion protein was identified by bright green MT bundling and/or other aggregates of bright green GFP protein, whereas overexpression of the EB1-GFP fusion protein was identified by the presence of bright green GFP protein throughout the MT network. Cells that clearly overexpressed high levels of either fusion protein were not included in these analyses.

Nocodazole Regrowth Assays

Nocodazole (Sigma-Aldrich) was prepared as a 33 mM solution in dimethyl sulfoxide (DMSO) and stored at −20°C. For nocodazole treatment, cells were incubated in growth medium supplemented with 33 μM nocodazole for 1 h at 37°C. Coverslips were rinsed two times in phosphate-buffered saline (PBS) (at room temperature), and a full volume of prewarmed growth medium was added to each sample. Coverslips were fixed at time points by immersion in ice-cold methanol. MTs were labeled by indirect immunofluorescence (described below). To quantify the MT aster growth after nocodazole washout, MT length from the centrosome was measured using the Zeiss LSM 510 imaging software.

Ad Stocks

The AdNull vector, a replication-deficient (E1-, E3-) serotype 5 Ad vector (Ad5) was a generous gift from Dr. Phil Leopold (Weill Medical College, Cornell University, Ithaca, NY). The AdNull vector was propagated in 293 cells (Graham *et al*., 1977). Virus particles were purified from cell lysates using a CsCl gradient (Rosenfeld *et al*., 1992), dialyzed against 0.01 M Tris-HCl, pH 7.8, 3% sucrose, 0.15 M NaCl, and 0.01 M $MgCl_2$, and stored at −70°C in 50-μl aliquots. Virus particle concentration (vp/ml) was calculated by measuring the A_{260} and dividing by the extinction coefficient for wild-type Ad ($\varepsilon_{260} = 9.09 \times 10^{-13}$ OD·ml·cm·virus particle^{-1}; Mittereder *et al*., 1996).

HHV-8 Stocks

Vero cells containing latent HHV-8 (rKSHV.219) were generously provided by Dr. Jeffrey Vieira (University of Washington, Seattle, WA). The production of infectious HHV-8 was induced by treatment with 1.25 mM sodium butyrate and a baculovirus expressing the HHV-8 RTA gene (Back50) as described previously (Vieira and O'Hearn, 2004). Briefly, after two rinses with PBS, the induction medium was replaced with serum-free medium at 24 h postinduction. An HHV-8 inoculum was harvested at 48 h postinduction and frozen at −80°C. The titer of the inoculum was estimated to be ~10^5 infectious units/ml as measured on 293 cells (Vieira and O'Hearn, 2004).

Conjugation of Fluorescent Dye to Ad Particles

The Alexa Fluor 555 carboxylic acid, succinimidyl ester (Invitrogen) was conjugated to our replication-deficient Ad5 stock using a protocol similar to that described previously (Leopold *et al*., 1998). Briefly, 100 μl of DMSO was added to 1 mg of the lyophilized Alexa Fluor dye. Our Ad5 stock was diluted to 10^{12} vp/ml in 0.1 M sodium bicarbonate buffer, pH 8.4, and the entire 100 μl of dye was added to 2 ml of diluted virus stock while the solution was mixed by vortexing. The reagents were mixed continuously by vortex for 1 h at room temperature in a foil-wrapped 15-ml tube. After the 1-h incubation, the entire 2-ml volume was injected into a 10-kDa MWCO Slide-A-Lyzer dialysis cassette (Pierce Chemical, Rockford, IL) and dialyzed overnight at 4°C against a total of two changes of 0.1 M Tris-HCl, pH 7.8, 0.1 M $MgCl_2$, 1.5 M NaCl, and 10% glycerol. The dialyzed Ad-AF555 was adjusted to a final concentration of 30% glycerol and stored at −20°C in 20-μl aliquots. The final concentration of Alexa Fluor 555 dye was determined as described previously (Leopold *et al*., 1998). We refer to the labeled virus as Ad-AF555.

The specificity of Alexa Fluor 555 fluorescence to Ad particles was tested by colocalizing Ad-AF555 with virus particles stained with a monoclonal antibody to Ad (type 1, 2, 5, and 6) hexon protein (MAB8044; Chemicon International, Temecula, CA). A549 cells on coverslips were infected with Ad-AF555 at 10^{10} vp/ml for 1 h, fixed with −20°C methanol, and incubated with the anti-Ad primary antibody (1:500) followed by a goat-anti-mouse Alexa Fluor 633 secondary antibody (1:200). Laser scanning confocal imaging revealed distinct colocalization of red and far-red fluorescence (our unpublished data), indicating that the Alexa Fluor 555 signal was due to the presence of Ad particles.

To test whether aggregated, uninfectious viral proteins labeled by the fluorophore were readily internalized by cells, we heated an aliquot of the fluorescently labeled virus preparation to 70°C for 30 min, conditions sufficient to render the Ad uninfectious (Maheshwari *et al*., 2004). We then incubated the heat-killed virus with HFF cells for 24 h, fixed the cells in methanol, and analyzed the cells for the presence of internalized AF-555 fluorescence. Large, apparently aggregated clusters of bright fluorescence were bound to the surface of some cells, although no Ad-associated fluorescence was internalized under these conditions. We did not observe the typical punctate distribution of internalized Ad-associated fluorescence after incubation with the heat-killed, fluorescently labeled Ad inoculum.

Infection of Cells with Fluorophore-labeled Ad5

Monolayers of A549 cells or HFF cells were grown on glass coverslips in six-well plates to ~50% confluence. For infection experiments, culture medium was replaced with fresh infection medium containing Ad-AF555 at a concentration of 10^{10} vp/ml. The approximate multiplicity of infection (MOI) was typically on the order of 10^4 vp/cell, although the actual MOI was lower due to limits on viral diffusion to the cell surface. After the specified infection times, cells on coverslips were rinsed once in prewarmed PBS and immediately fixed in −20°C methanol for 10 min. For live-cell microscopy with Ad-AF555, cells on coverslips were incubated with Ad for the indicated time, transferred to the imaging chamber, and loaded with virus-free media to minimize the nonspecific fluorescence from unbound Ad-AF555 particles. Using high MOI infection conditions (10^4 virus particles/cell), every cell contained several Ad particles that were easily detected by the punctate distribution of bright red AF555 fluorescence (our unpublished data).

Rho Activity Assays

A commercially available, enzyme-linked immunosorbent assay (ELISA)-based RhoA activity assay (G-LISA; Cytoskeleton, Denver, CO) was used to measure the relative RhoA activity of serum-starved HFF cells after experimental treatments. Whole cell lysates were processed as per the G-LISA protocol using lysis buffer provided in the kit. The lysates were incubated in microwells to which the rhotekin binding domain peptide was bound, and active RhoA was detected using indirect immunodetection followed by a colorimetric reaction measured by absorbance at 490 nm.

Inhibition of RhoGTPases

Inhibition of RhoA was achieved by pretreatment of cells with *Clostridium botulinum* exoenzyme C3 (Cytoskeleton) at a concentration of 10 μg/ml (Aikawa *et al*., 1999; Alblas *et al*., 2001). Rac1 was inhibited by pretreating HFF cells with NSC23766 (EMD Biosciences, San Diego, CA) at 100 μM for 2 h. NSC23766 inhibited Rac1 activity by blocking the interaction between Rac1

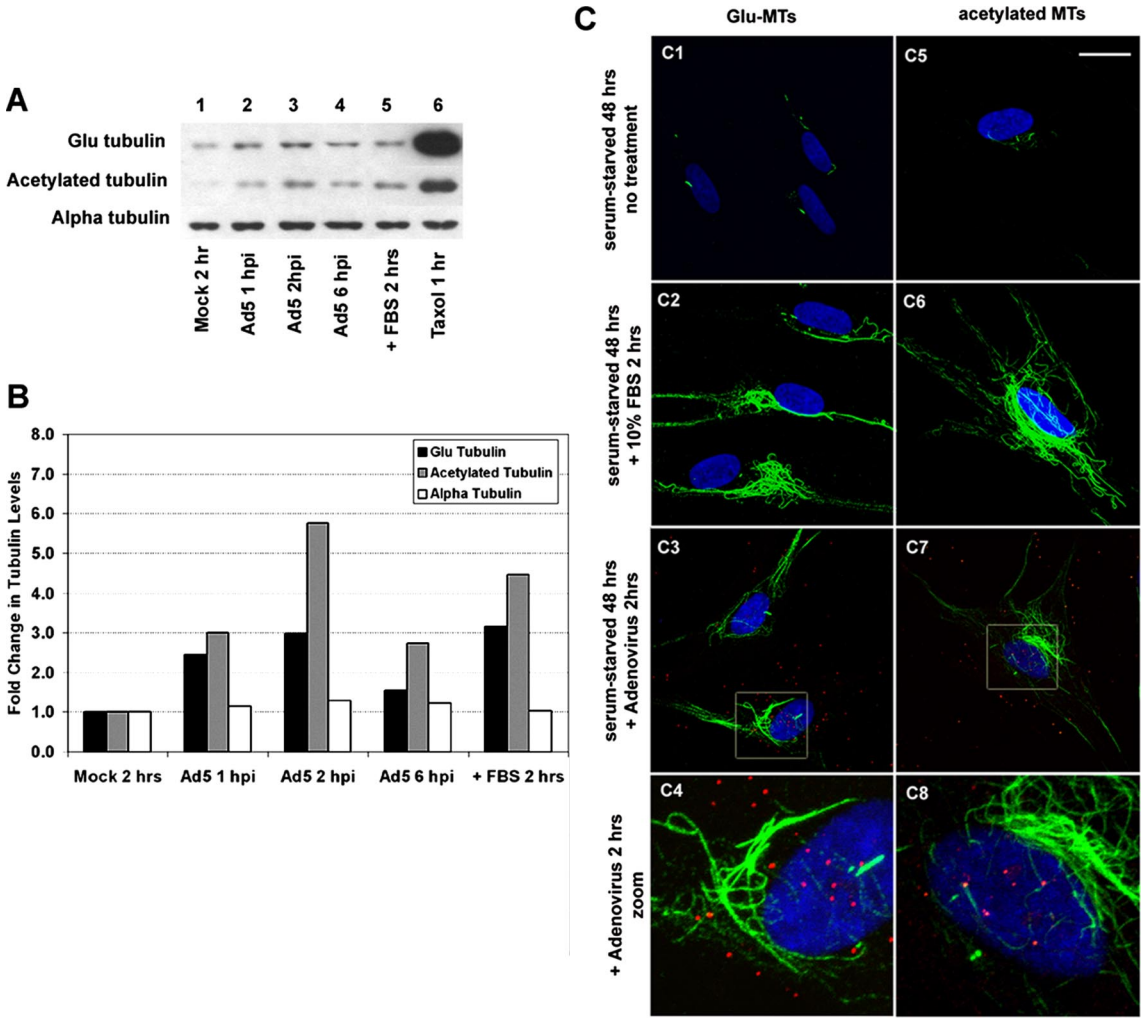

Figure 1. Ad infection results in increased levels of posttranslationally modified tubulin in serum-starved HFF cells. (A) HFF cells were grown in serum-free media for 48 h and then mock infected for 2 h (lane 1), infected with Ad for the indicated times (lanes 2–4), treated with 10% FBS for 2 h (lane 5), or treated with 5 μM taxol for 1 h (lane 6). (B) Immunoblots were quantified by densitometry, and the values were normalized to the mock-infected condition. (C) HFF cells were serum-starved for 48 h and subsequently incubated under the indicated conditions for an additional 2 h. Fixed cells were labeled with antibodies against detyrosinated tubulin (Glu-MTs; green, C1–C4) or acetylated tubulin (green, C5–C8). Nuclei (blue) were stained with TO-PRO-3 iodide. Serum starvation depleted most Glu-MTs (C1) and acetylated MTs (C5), and these recovered after incubation with 10% FBS (C2 and C6). By 2 h postinfection, Ad-treated cells exhibited substantial increases in both Glu-MTs (C3) and acetylated MTs (C7). Regions defined in C3 and C7 were enlarged to more clearly define the Ad-associated fluorescence (red). Bar, 20 μm.

and its guanine nucleotide exchange factors TrioN and Tiam1 (Gao *et al.*, 2004). At 100 μM, NSC23766 specifically inhibited platelet-derived growth factor (PDGF)-induced Rac1 activity in fibroblast cells without inhibiting the activity of RhoA or CDC42 (Gao *et al.*, 2004). This inhibition was also sufficient to block Rac1-mediated lamellipodia formation and cell proliferation in response to PDGF in fibroblast cells (Gao *et al.*, 2004).

Indirect Immunofluorescence

Immunofluorescence of cells on coverslips was performed as described previously (Piehl and Cassimeris, 2003). Primary antibodies used were mouse anti-α-tubulin (B512, 1:1000; Sigma-Aldrich), mouse anti-Ad type 1, 2, 5, and 6 hexon (MAB8044, 1:500; Chemicon International), rabbit anti-γ-tubulin (AK-15, 1:1000; Sigma-Aldrich), mouse anti-acetylated tubulin (6-11B-1, 1:250; Sigma-Aldrich) and rabbit anti-Glu (detyrosinated)-tubulin (AB3201, 1:250; Chemicon International). Secondary antibodies used were goat-anti-mouse or goat-anti-rabbit Alexa Fluor 488, 563, or 633 (1:200; Invitrogen).

Immunoblot Analysis

Cytoskeleton and soluble fractions were prepared from cell lysates as described previously (Howell *et al.*, 1999). Briefly, cells were lysed in an MT stabilization buffer: PEM (100 mM PIPES, pH 7.6, 2 mM EDTA, and 1 mM $MgSO_4$) containing 0.5% NP-40, 4 nM paxlitaxel (Sigma-Aldrich), 15% glycerol, and 1× protease inhibitor cocktail (Roche Diagnostics). Lysates were clarified by centrifugation at 13,000 × *g* for 10 min, and pellets containing polymerized MTs were resuspended in MT stabilization buffer. The resuspended pellets were diluted in PAGE sample buffer, resolved in 10% polyacrylamide gels, and transferred to Immobilon membranes (Millipore, Billerica, MA). Nonspecific binding to the membrane was blocked with 5% nonfat milk in Tris-buffered saline, 0.2% Tween 20. Membranes were probed with primary antibodies followed by secondary antibodies conjugated to horseradish peroxidase. Immunoreactive bands were developed by enhanced chemiluminescence (PerkinElmer Life and Analytical Sciences, Boston, MA) according to the manufacturer's specifications.

Confocal Microscopy

Laser scanning confocal imaging was performed as described previously (Piehl and Cassimeris, 2003). In short, images were acquired using a 63× numerical aperture 1.4 PlanApo differential interference contrast (DIC) objective on an inverted microscope (Axiovert 200M; Carl Zeiss, Jena, Germany) equipped with an LSM510META scan head (Carl Zeiss). Argon ion (488), 543 HeNe, and 633 HeNe lasers were used to generate the excitation lines, and multitrack sequential excitation was used to avoid bleed-through between

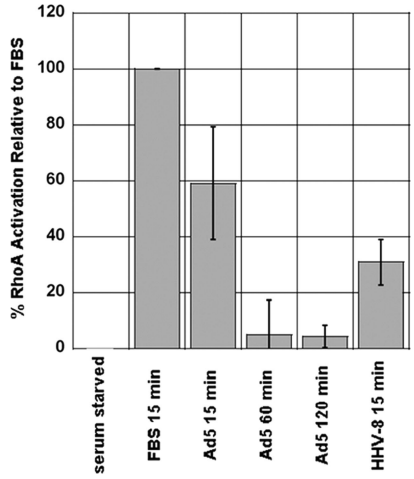

Figure 2. Ad infection is accompanied by a transient activation of RhoA that occurs within 15 min of infection. A_{490} values from the colorimetric GLISA assay were normalized by calculating the percentage of activation relative to serum-starved samples. The percentage of activation of the FBS control was assigned a value of 100, and the percentage of activation of virus-treated samples was normalized relative to the FBS control. Each data point represents the mean activation value from three to six individual assays ±SEM.

fluorophores. For the analysis of Ad-AF555 distribution within A549 and HFF cells, three-color 512 × 512 images were acquired using two-line mean averaging in a Z-series typically containing 15–25 overlapping stacks of 0.74-μm sections. Three color Z-stacks were then converted to two-dimensional projections using the LSM510-META software (Carl Zeiss). Ad-AF555 localization to the nucleus or centrosome was determined by its respective colocalization with TO-PRO-3 iodide (Invitrogen) or γ-tubulin.

For live-cell imaging, coverslips were housed in a POC-mini imaging chamber (Carl Zeiss) and loaded with prewarmed DMEM (without phenol red; Invitrogen) supplemented 0.3 U/ml Oxyrase oxygen scavenging system (Oxyrase, Mansfield, OH) to minimize photodamage. The POC-mini chamber was maintained at 37°C on the microscope stage using both stage and objective heaters (Heating Insert P; Carl Zeiss). Each coverslip was examined for no more than 1 h. To image EB1-GFP and measure MT nucleation rate, 10–20 images were acquired every 2 s using four-line mean averaging, requiring a scan time of 1.9–2.0 s. Usually three time-lapse series were acquired for each cell for a total imaging time of 60–120 s/cell. To image MT dynamics in cells expressing GFP-tubulin, 10–20 images were acquired every 4 s using four-line mean averaging requiring a scan time of 3.9–4.0 s.

Image Analysis and Microtubule Tracking

MetaView imaging software (Molecular Devices, Sunnyvale, CA) was used to track the number and position of virus-associated fluorescence within two-dimensional projections of confocal image stacks. To measure Ad-AF555 subcellular distributions, independent measurements of the total red fluorescence intensity (due to Ad-AF555), red fluorescence of a single punctate AF555 spot, nuclear red fluorescence, centrosomal red fluorescence, and background red fluorescence were obtained for each cell. The background fluorescence was subtracted for each region, and the fluorescence intensity for each region was normalized to the intensity of a single Ad-AF555 fluorescent spot. As a result, the number of distinct red fluorescent spots was quantified as a function of their spatial distribution throughout the cell.

The MetaView software was also used to track the length changes of individual MTs at the periphery of cells expressing GFP-tubulin (Rusan *et al*., 2001). The selection of individual MTs for tracking was based on our ability to clearly define a plus-end tip for at least a 12-s interval. The mean tracking duration for individual MTs was 45 ± 15 s, and all clearly defined MTs within an image series were tracked.

Dynamic Instability Calculations

The change in length over time, i.e., the growth and shortening rates, were calculated for each MT tracked as well as the total time spent in growth, shortening, or pause. MT pause was defined as a change in distance of <0.25 μm over a 4-s time frame. Dynamicity was calculated for each MT by adding the total growth length and the total shortening length and dividing by the total imaging time. Drift velocity (Vorobjev *et al*., 1999) was calculated for each MT by subtracting the total shortening length from the total growth length and dividing by the total imaging time. Transition frequencies were calculated as the number of catastrophes (k_c) or rescues (k_r) per unit time (seconds). The standard deviations for transition frequencies were calculated as described by Howell *et al*. (1999).

RESULTS

Ad Infection Increases the Level of Posttranslationally Modified Tubulin within Host Cells

Most mammalian cells contain both dynamic and differentially stable subsets of MTs (Webster *et al*., 1987). The stable population of MTs are easily identified by immunofluorescence using antibodies recognizing detyrosinated (Gundersen *et al*., 1994) or acetylated (Matsuyama *et al*., 2002) tubulin. A recent study has indicated that HHV-8 binding to cellular

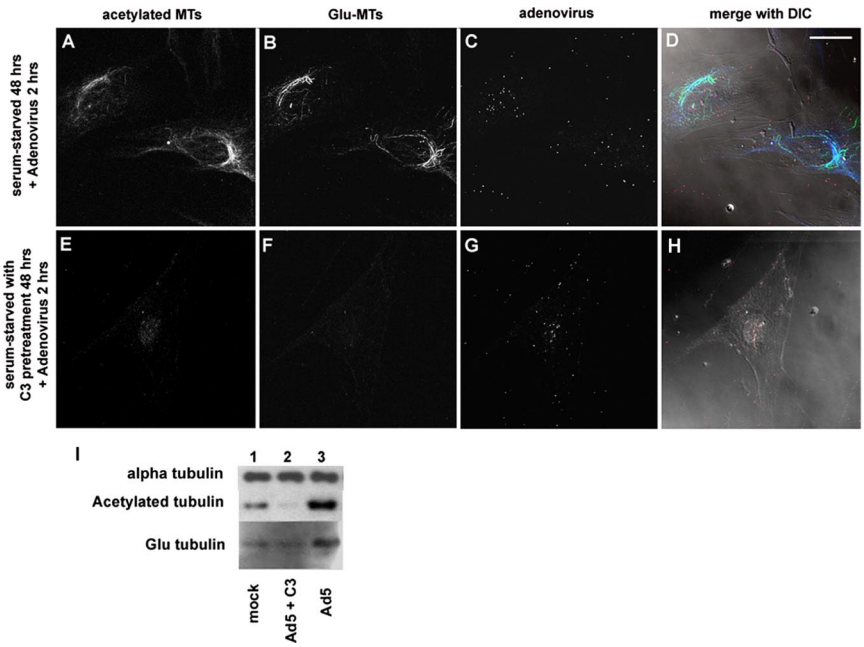

Figure 3. Elevated levels of posttranslationally modified MTs after Ad infection require the activity of RhoA. Serum-starved HFF cells infected with fluorophore-labeled Ad were either untreated (A–D) or pretreated with 10 μg/ml *C. botulinum* exoenzyme C3 for 48 h (E–H) to inhibit RhoA activity. Untreated cells infected with Ad for 2 h contain substantial levels of acetylated MTs and Glu-MTs (A–D). Cells pretreated with the RhoA-inhibitor C3 did not accumulate readily detectable acetylated or Glu MTs (E–H). Ad-associated fluorescence occurs as white spots on the black background (C and G). The fluorescent images were merged with DIC images (E and H) to define cellular boundaries. Bar, 20 μm. (I) Immunoblots of posttranslationally modified tubulin confirm that C3 pretreatment blocks the Ad-induced increase in tubulin acetylation and Glu-tubulin. The levels of α-tubulin remain relatively unchanged.

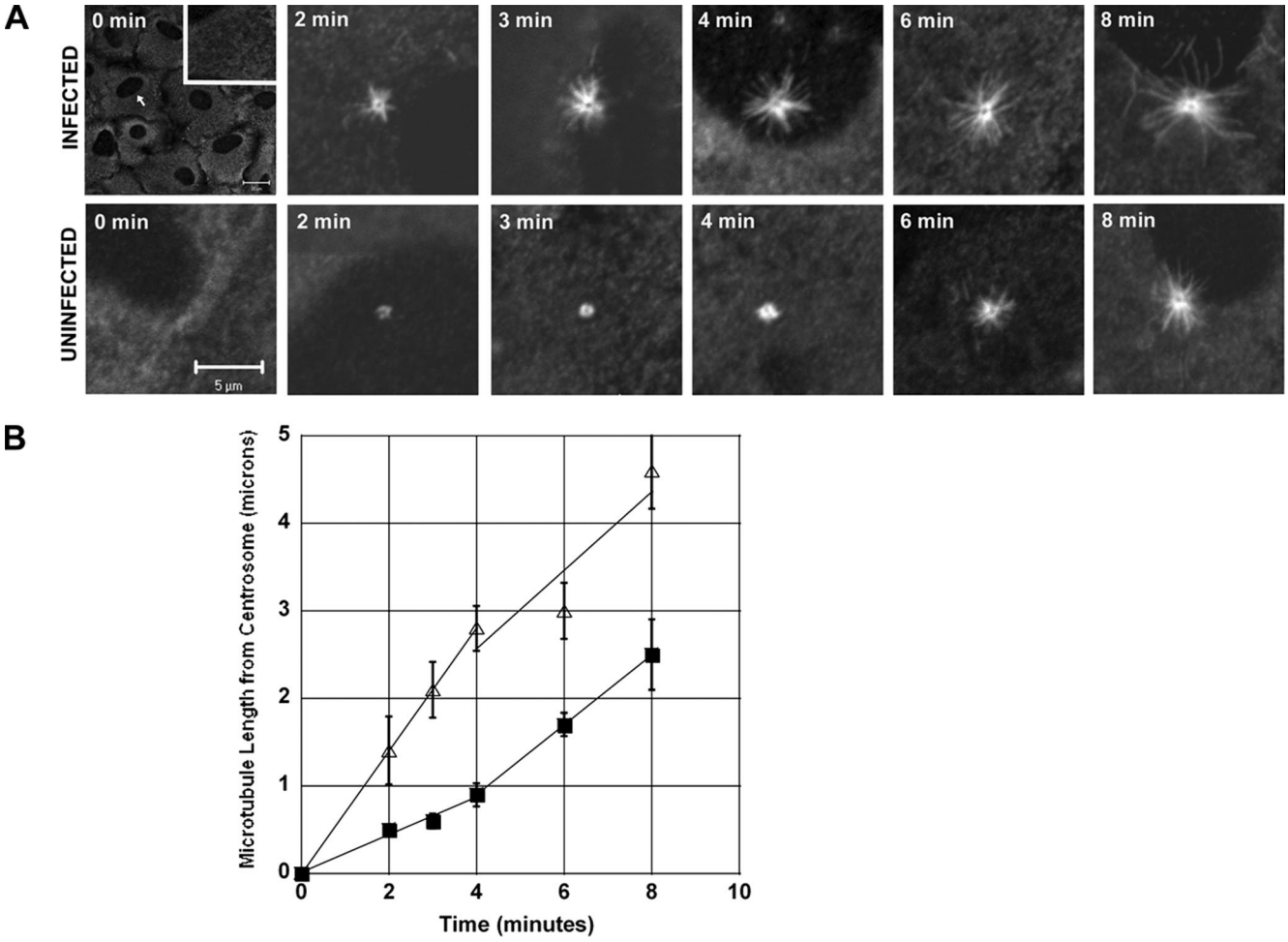

Figure 4. MT regrowth after nocodazole washout is faster in Ad-infected cells compared with uninfected cells. (A) The size of MT asters increased over time after nocodazole washout in uninfected cells (bottom) or cells infected with Ad for 10 min before nocodazole treatment (top). A549 cells were incubated with Ad for 10 min at 37°C and then treated with 33 μM nocodazole for 60 min at 37°C. Cells were washed two times in PBS to remove nocodazole and subsequently incubated in fresh, prewarmed medium for the indicated times. (B) The rate of MT growth after nocodazole washout is higher in cells infected with Ad for 10 min before nocodazole treatment (△) compared with uninfected controls (■). Each point is the average of 10 measurements ±SD.

integrins results in a Rho-GTPase–mediated increase in the acetylation of host cell MTs (Naranatt *et al*., 2005). Considering that Ad infection involves similar association with host cell integrins (Wickham *et al*., 1993), we used immunofluorescence and immunoblotting techniques to determine whether Ad infection modified the levels of posttranslationally modified tubulin within host cells.

Serum-starved HFF cells were infected with fluorescently labeled Ad (Ad-AF555) at a concentration of 10^{10} vp/ml for 1, 2, and 6 h and subsequently analyzed by fluorescence microscopy and immunoblotting to measure the levels of detyrosinated MTs (Glu-MTs) and acetylated MTs. Immunoblots revealed that Ad-infected cells contained substantially higher levels of both Glu-tubulin and acetylated tubulin (Figure 1A, lanes 2–4) compared with uninfected cells (Figure 1A, lane 1). Quantitation of immunoblots revealed that cells infected for up to 2 h contained two- to threefold more Glu-tubulin and three- to sixfold more acetylated tubulin than uninfected cells. The induction of posttranslationally modified tubulin observed in Ad-infected cells was similar to results observed following incubation for 2 h in 10% FBS (Figure 1, A and B). Results of microscopic observations were consistent with immunoblot results (Figure 1C).

Ad-infected Cells Exhibit Elevated Levels of Active RhoA

The accumulation of Glu-MTs in serum-starved fibroblasts is regulated by the activation of the RhoGTPase RhoA and its downstream effector mDia, which associates with MT plus-end binding proteins to "cap" the MT plus end and stabilize MT dynamics (Infante *et al*., 2000; Palazzo *et al*., 2001; Wen *et al*., 2004). The molecular mechanisms regulating acetylation of MTs is less clearly understood, although activation of RhoA has been implicated in the HHV-8–induced hyperacetylation of MTs (Naranatt *et al*., 2005). To determine whether Ad infection of serum-starved HFF cells was accompanied by activation of RhoA, we used a commercially available RhoA activation ELISA assay (G-LISA; Cytoskeleton). HFF cells grown on 100-mm plates were serum starved for 24–48 h before these experiments. Cells were then treated with Ad (10^{10} particles/ml) at 37°C for 15, 60, or 120 min. As a positive control for RhoA activation, cells were treated with 10% FBS for 15 min. For each color-

imetric assay, A_{490} values from Ad-treated cell lysates were normalized to the A_{490} values from FBS-treated cell lysates, which were assigned a value of 100% activation. Elevated levels of active RhoA relative to serum-starved conditions were detected in each of the Ad-infected cell lysates (Figure 2). The level of RhoA activation in Ad-infected cells was 60% (relative to FBS-treated cells) by 15 min postinfection, and by 60 and 120 min postinfection this level had decreased to below 20% (Figure 2). To compare the magnitude of Ad-induced RhoA activation in these experiments, we also treated serum-starved HFF cells with HHV-8, a known activator of RhoA (Naranatt *et al*., 2005). The level of RhoA activation in HHV-8–treated cells at 15 min postinfection was similar to levels seen in Ad-treated cells (Figure 2).

Inhibition of RhoA by C3 Exoenzyme Reduced Levels of Ad-induced Acetylation and Detyrosination of Host Cell MTs

To determine whether RhoA activation was necessary for the Ad-induced increases in MT acetylation or detyrosination, we pretreated serum-starved HFF cells with *C. botulinum* exoenzyme C3, which specifically inactivates RhoA but does not inhibit the activity of other RhoGTPases such as Rac1 or CDC42. HFF cells were serum-starved for 48 h, and a subset of cultures were pretreated with C3 exoenzyme at a concentration of 10 μg/ml during the 48-h serum starvation period. Some cultures were then treated with Ad at a concentration of 10^{10} particles/ml at 37°C for 2 h, and the levels of posttranslationally modified tubulin were analyzed by immunofluorescence and immunoblotting. Microscopic analyses of infected cells revealed the presence of both acetylated and detyrosinated MTs (Figure 3, A and B), whereas cells pretreated with C3 had greatly reduced numbers of acetylated or detyrosinated MTs (Figure 3, E and F). Ad-associated fluorescence was detected in both C3-treated cells (Figure 3G) and untreated cells (Figure 3C), indicating that viral entry was not blocked by C3 treatment. Immunoblotting of cytoskeletal fractions confirmed that treatment with C3 exoenzyme abrogated the increase in acetylated and detyrosinated tubulin normally observed by 2 h postinfection (Figure 3I).

MTs become acetylated either as a consequence of stabilization or by manipulation of the primary tubulin deacetylase HDAC6 (Hubbert *et al*., 2002). In the latter case, MT hyperacetylation may occur without altering MT dynamics (Palazzo *et al*., 2003). Acetylation of MTs is therefore not necessarily a direct indicator of MT stability. The next series of experiments were designed to systematically characterize the extent to which Ad infection alters the dynamic instability of host cell MTs.

Rate of MT Regrowth after Nocodazole Washout Is Higher in Ad-infected Cells Compared with the MT Regrowth Rate in Uninfected Cells

As an initial assessment of MT dynamics, we measured the rate of MT regrowth after removal of nocodazole. Significant Ad-induced alterations in the actin cytoskeleton have been observed in A549 cells as soon as 10 min postinfection (Li *et al*., 1998a), and as such we chose this time frame for our initial regrowth experiments. Cells were treated with Ad and 33 μM nocodazole as described in *Materials and Methods* and then fixed at 0–8 min after nocodazole washout. The MT network of infected and uninfected A549 cells was completely depolymerized after the 1-h incubation in nocodazole (Figure 4A). MT asters formed within minutes of nocodazole washout, and it was apparent that MT asters grew faster in infected cells compared with those in uninfected cells. Within the first 4 min after nocodazole washout, the rate of MT regrowth was threefold faster in the Ad-infected cells compared with that in uninfected cells (Figure 4B). Infected and uninfected cell MTs grew at similar rates during 5–8 min post nocodazole washout, but by 8 min the asters in infected cells were on average twice the size of those in uninfected cells.

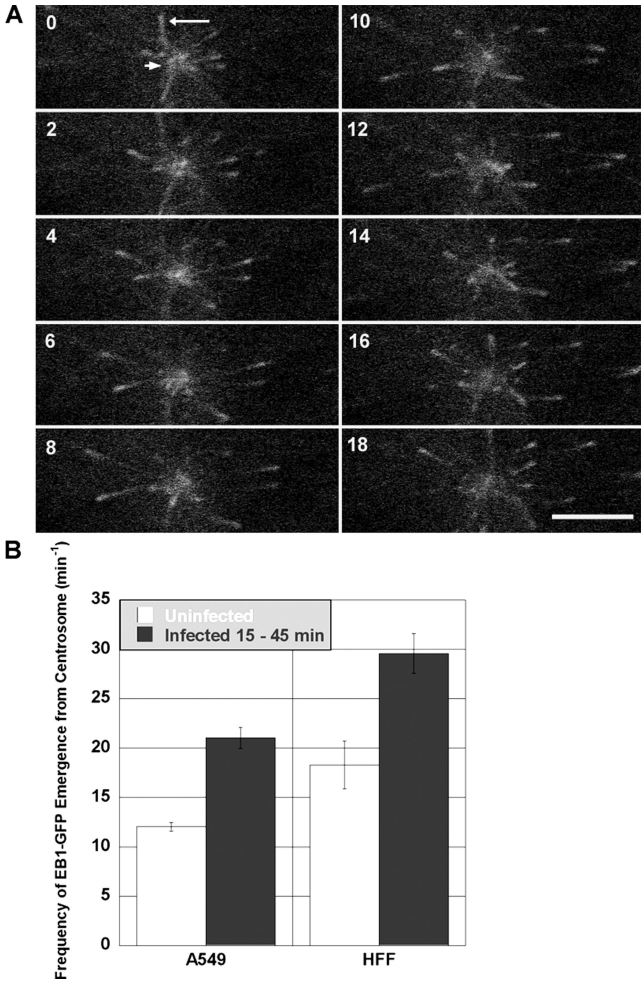

Figure 5. Live cell analysis of EB1-GFP emergence from the centrosome. (A) EB1-GFP was detected as bright fluorescent spots (long arrow) emanating from the centrosome (short arrow) over time (seconds). Bar, 5 μm. (B) MT nucleation rate was measured by the frequency of EB1-GFP comet emergence from the centrosome over time (minute^{-1}). Cells infected for 15–45 min with Ad (dark bars) exhibited a significantly higher rate of MT nucleation compared with uninfected cells (white bars) in both A549 cells ($p = 3 \times 10^{-11}$) and HFF cells ($p = 1 \times 10^{-7}$). Each bar represents the mean frequency from 20 to 40 distinct measurements per condition ±SEM.

These initial experiments demonstrated that a 10-min incubation with Ad (followed by a 1-h postinfection treatment with nocodazole) resulted in an increased rate of MT regrowth after nocodazole washout. Assuming that this observed difference in MT growth from the centrosome could be due to factors directly or indirectly affecting either MT growth rate or MT nucleation events, we conducted live cell analyses to test both processes.

Ad Infection Enhances the Frequency of MT Nucleation at the Centrosome

Virus infection has previously been implicated in altering host cell MT nucleation efficiency (Ploubidou *et al*., 2000). In

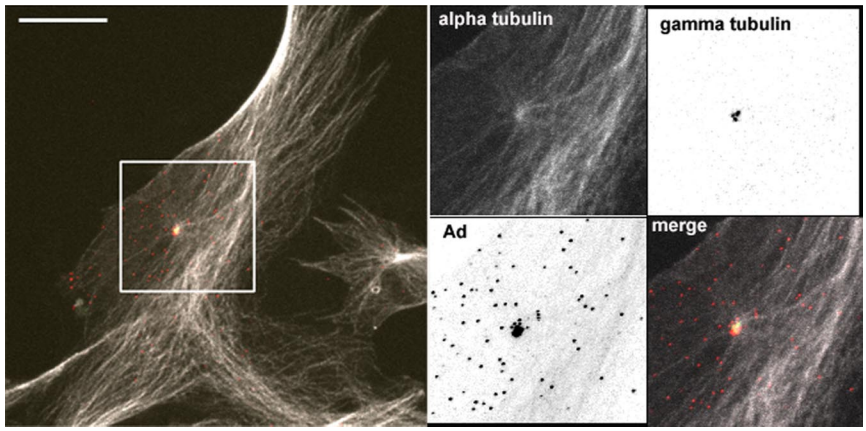

Figure 6. HFF cell infected with Ad-AF555 for 24 h. An accumulation of several Ad-AF555 fluorescent units colocalized with γ-tubulin at the centrosome in many cells, and the remaining Ad-associated fluorescence was evenly distributed among nuclear and cytoplasmic regions. Images of γ-tubulin and Ad were inverted for clarity, and the corresponding fluorescence occurs as black spots on a white background. Bar, 20 μm.

this previous study, infection of HeLa cells for 2 h with vaccinia virus reduced the efficiency with which MTs regrew after nocodazole washout. To more specifically examine the effect of Ad infection on MT nucleation at the centrosome, we transiently expressed GFP-EB1 in A549 and HFF cells and acquired a series of images from living cells. GFP-EB1 binds to MT tips and fluorescent EB1 "comets" emerge from the centrosome as new MTs are nucleated (Figure 5A; Piehl *et al.*, 2004). The number of EB1 comets emerging from the centrosome over time (nucleation frequency) was counted for both uninfected and infected A549 and HFF cells. As shown in Figure 5B, the MT nucleation frequency of Ad-infected A549 cells increased by 75% compared with the MT nucleation frequency of uninfected A549 cells. This trend was also observed in the HFF cell line, in which the MT nucleation rate increased by >60% in infected HFF cells compared with uninfected HFF cells.

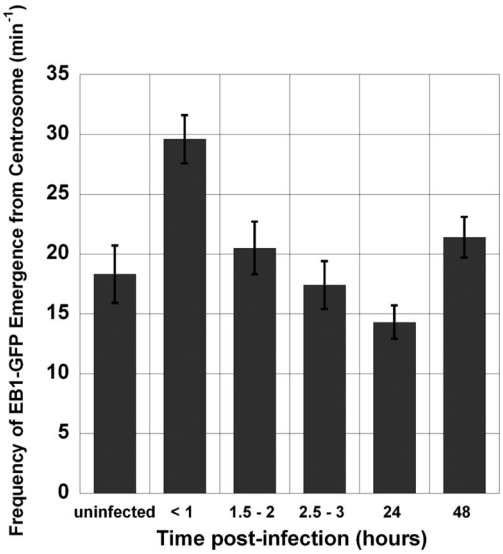

Figure 7. Ad-induced enhancement in MT nucleation recovers to uninfected levels by 1.5 h postinfection. MT nucleation was visualized by live-cell imaging of EB1-GFP expression in HFF cells after infection with Ad-AF555 for the indicated times. Ad infection results in a transient enhancement in MT nucleation frequency within 1 h postinfection. The nucleation frequency in cells infected for 24 h was significantly lower ($p < 0.05$) compared with the same measurement in uninfected cells, although this trend was not observed in cells infected for 48 h. Each value represents the mean ± SEM of 16–50 individual live-cell measurements.

Localization of Ad at the Centrosome Does Not Enhance MT Nucleation

We next examined whether the spatial localization of Ad within the cell could affect the frequency of MT nucleation at the centrosome. Previous studies indicated that Ad accumulates at the centrosome within an hour of infection (Glotzer *et al.*, 2001), which is within the time frame we used to measure MT nucleation. This observation raised the possibility that Ad transport to the centrosome could influence MT nucleation. To address this issue, we examined Ad localization in A549 and HFF cells. As expected, Ad-associated fluorescence localized to the nuclear region of A549 cells within an hour postinfection, and the nuclear localization of Ad became enriched and more clearly defined with increased time postinfection (see Supplemental Material). We did not detect Ad-associated fluorescence at the centrosome of A549 cells. In contrast, infected HFF cells showed clear centrosomal localization of up to 30% of the Ad-associated fluorescence within 2–24 h postinfection (Figure 6 and Supplemental Figure S1).

Considering that Ad-AF555 localized to the centrosome in HFF cells (Figure 6), we investigated whether this centrosomal accumulation of virus affected MT nucleation. HFF cells were transfected with EB1-GFP plasmid and subsequently incubated with Ad-AF555 at a concentration of 10^{10} vp/ml. MT nucleation rate was measured by EB1-GFP comet emergence from the centrosome after 2, 3, 24, and 48 h of infection. As expected, many infected cells had distinct foci of bright red Ad-AF555 fluorescence that colocalized with the EB1-GFP fluorescence at the centrosome. Despite the frequent localization of Ad at the centrosome at >2 h postinfection, we did not observe a corresponding enhancement in MT nucleation frequency under these conditions (Figure 7). These data indicate that extended infection time and continued minus-end delivery of Ad cargo did not directly affect MT nucleation frequency.

Ad Infection Increased the Percentage of Time MTs Spent in Growth and Decreased MT Catastrophe Frequency

A significant increase in MT nucleation frequency was observed within an hour postinfection, and as such we chose the same infection time period to analyze all parameters of MT plus-end dynamic instability within infected cells. A549 and HFF cells were first transfected with a plasmid expressing GFP-tubulin (Figure 8) and then infected with Ad-AF555. MTs were highly dynamic in both infected and uninfected cells, as indicated by the mean dynamicity values of 9.5–11.4 μm/min (A549 cells; Table 1) and 12.6–13.5 μm/min (HFF cells; Table 2).

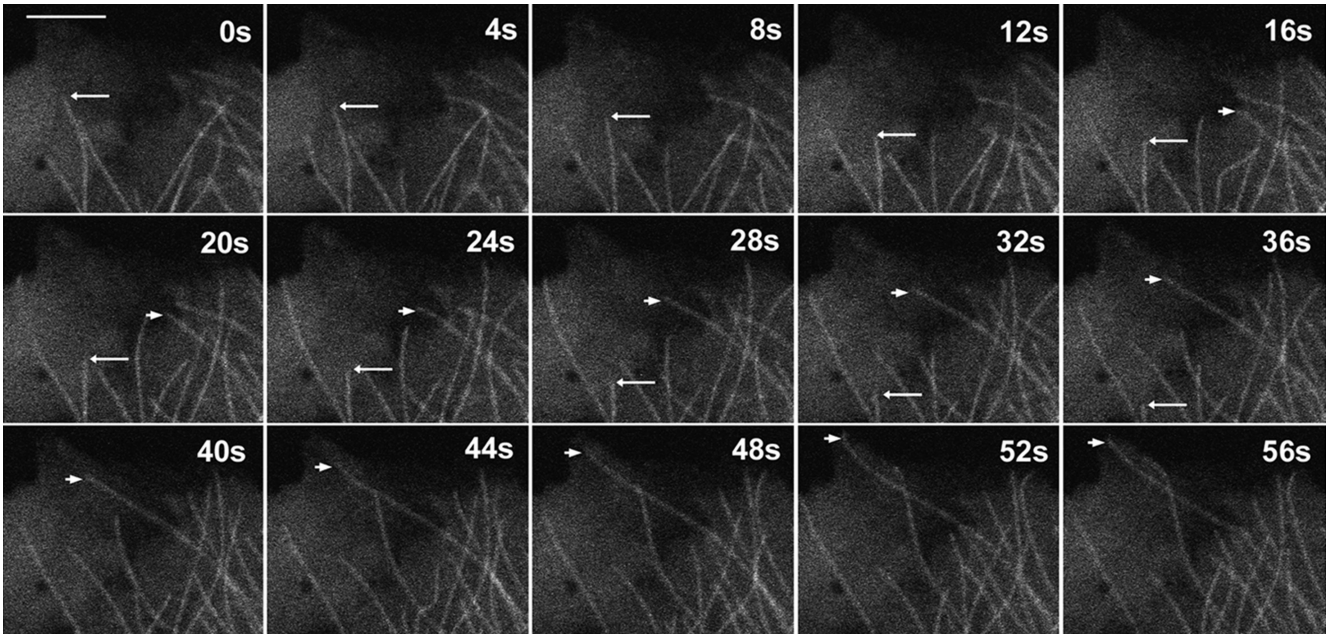

Figure 8. Dynamic instability of individual MTs at the cell periphery. Images from the periphery of live A549 cells expressing GFP-α-tubulin were acquired every 4 s to capture the dynamic transitions of individual MTs. An example of MT shortening is indicated by the long arrow, and MT growth is indicated by the short arrow. Bar, 5 μm.

As expected, the measured parameters of dynamic instability for individual MTs were highly variable, indicated by the standard deviations shown in Tables 1 and 2. Despite this variability, several significant differences were identified between the dynamics of MTs in Ad-infected cells and those in uninfected cells. The mean drift velocity (Vorobjev *et al*., 1999), which defines the overall net gain or loss of MT polymer over time, was found to be significantly higher under infected conditions in both A549 cells (Table 1) and HFF cells (Table 2). The positive drift velocity measured in infected cells indicates that the dynamics of MTs at the periphery of these cells are shifted toward net growth, whereas drift velocity in uninfected cells is closer to zero, reflecting a balance between overall growth and shortening. The mean growth rate and dynamicity values of MTs were significantly higher in infected A549 cells compared with uninfected cells, although these trends were not similarly significant in HFF cells.

Table 1. MT dynamic instability parameters in uninfected or Ad-infected A549 cells

	A549 cells	
Parameter	Uninfected	Infected
Total no. of MTs	139	124
Total time tracked (s)	5350	5039
Parameters of dynamic instability		
Growth rate (μm/min)	11.2 ± 5.9	13.9 ± 7.3*
Net growth/MT (μm)	3.0 ± 2.5	4.5 ± 3.3*
Shortening rate (μm/min)	13.0 ± 7.1	11.9 ± 7.0
Net shortening/MT (μm)	2.7 ± 1.9	2.1 ± 2.0*
% time spent in growth	34.2	40.4
% time spent in shortening	29.7	22.6
% time spent in pause	38.7	38.6
Dynamicity (μm/min)	9.5 ± 5.4	11.4 ± 6.6*
Drift velocity (μm/min)	0.7 ± 7.6	4.9 ± 8.3*
Transition frequencies (s^{-1})		
Catastrophe frequency	0.051 ± 0.004	0.039 ± 0.003*
Rescue frequency	0.048 ± 0.004	0.048 ± 0.004

MTs within Ad-infected cells spent more time in growth, less time in shortening, and exhibited significantly higher drift velocities and lower catastrophe frequencies. Confocal imaging and image analysis were performed to track the length changes of individual MTs and to calculate the parameters of MT dynamic instability as described in *Materials and Methods*. Mean data are presented ±SD. Statistically significant differences were identified using analysis of variance (ANOVA) single-factor analysis (growth rate, net growth, shortening rate, net shortening, dynamicity, and drift velocity) or Student's *t* test, two means with unequal variance (catastrophe and rescue frequencies).

* Mean values from infected cells are significantly different ($p < 0.05$) from corresponding values in uninfected cells.

In addition, MTs within Ad-infected cells spent a higher percentage of time in growth and less time in shortening compared with uninfected conditions in both cell lines. Specifically, infected A549 cell MTs spent ~18% more time in growth and 25% less time in shortening compared with the uninfected controls (Table 1). The difference in percentage of time in growth was identical in HFF cells, where infected cell MTs spent 18% more time in growth than uninfected controls (Table 2). Furthermore, MTs from infected HFF cells spent 43% less time in shortening compared with uninfected controls (Table 2). The differences in time distribution of MT dynamic instability among infected and uninfected cells reflected the trend identified by the drift velocity values, indicating a shift toward net growth and away from net shortening.

Analysis of the transition frequencies determined that MTs in infected cells exhibited lower catastrophe frequencies (k_c) compared with uninfected controls, and this trend was consistent in both cell lines. MTs in infected A549 cells underwent catastrophe 24% less often than uninfected conditions (Table 1), whereas the k_c in HFF cells was 46% lower in infected cells compared with uninfected controls (Table 2). The decrease in k_c observed in infected HFF cells was accompanied by a 16% increase in rescue frequency (k_r)

Table 2. Effects of Ad infection on the MT dynamic instability of Rac1-inhibited and noninhibited HFF cells

	HFF cells		Rac1-inhibited HFF cells	
Parameter	Uninfected	Infected	Uninfected	Infected
Total no. of MTs	69	61	90	93
Total time tracked (s)	3148	2488	4624	4936
Parameters of dynamic instability				
Growth rate (μm/min)	12.0 ± 6.7	11.6 ± 6.1	10.0 ± 5.1*†	7.3 ± 2.9*†
Net growth/MT (μm)	4.8 ± 2.7	5.1 ± 3.1	4.2 ± 2.0	2.8 ± 1.6*†
Shortening rate (μm/min)	14.8 ± 10	17.5 ± 14.1	13.4 ± 8.2	10.2 ± 5.8*†
Net shortening/MT (μm)	4.1 ± 3.8	2.6 ± 2.9*	3.7 ± 1.9	2.0 ± 1.2*
% time spent in growth	45.2	53.1	44.3	35.3
% time spent in shortening	30.6	17.5	28.9	19.1
% time spent in pause	25.3	29.4	27.3	45.6
Dynamicity (μm/min)	12.6 ± 5.4	13.5 ± 8.6	9.5 ± 4.0*†	5.5 ± 2.7*†
Drift velocity (μm/min)	−0.8 ± 7.2	3.1 ± 13.3*	−0.3 ± 3.7	0.5 ± 1.8†
Transition frequencies (s^{-1})				
Catastrophe frequency	0.052 ± 0.005	0.028 ± 0.004*	0.057 ± 0.004	0.052 ± 0.003†
Rescue frequency	0.061 ± 0.006	0.071 ± 0.008	0.071 ± 0.005	0.044 ± 0.004*†

Cells transiently expressing α-tubulin-GFP were either untreated (noninhibited HFF cells) or pretreated with NSC23766 (100 μM) for 2 h (Rac1-inhibited HFF cells). Confocal imaging and image analysis were performed to track the length changes of individual MTs and to calculate the parameters of MT dynamic instability as described in *Materials and Methods*. Mean data are presented ±SD. Statistically significant differences were identified using ANOVA single-factor analysis (growth rate, net growth, shortening rate, net shortening, dynamicity, and drift velocity) or Student's *t* test, two means with unequal variance (catastrophe and rescue frequencies). Rac1 inhibition reversed the Ad-induced pioneer MTs characteristics as indicated by three parameters. 1) Percentage of time spent in growth: In Rac1-inhibited HFF cells, MTs within Ad-infected cells spent less time in growth compared with uninfected cells. 2) Drift velocity: Rac1 inhibition abrogated the Ad-induced shift to net growth previously seen in noninhibited (Rac1-positive) cells. 3) Catastrophe frequency: Rac1 inhibition abrogated the Ad-induced decrease in catastrophe frequency previously seen in noninhibited (Rac1-positive) cells.

* Infected versus uninfected comparison: mean values from infected cells are significantly different ($p < 0.05$) from corresponding values in uninfected cells.

† Rac1-inhibited versus noninhibited comparison: Mean values from Rac1-inhibited cells are significantly different ($p < 0.05$) from respective values in noninhibited cells.

compared with uninfected HFF cells, although this trend was not observed in A549 cells. Analysis of the dynamic instability parameters and the transition frequency data indicates that Ad infection confers an overall stabilizing effect on the dynamic population of MTs at the periphery of infected cells.

The Ad-induced Shift in Dynamic Instability Requires the Activity of Rac1

MTs at the periphery of Ad-infected cells underwent a shift in dynamics that included three parameters: a low catastrophe frequency (k_c), increased time spent in growth, and a positive drift velocity, indicating a bias toward net growth.

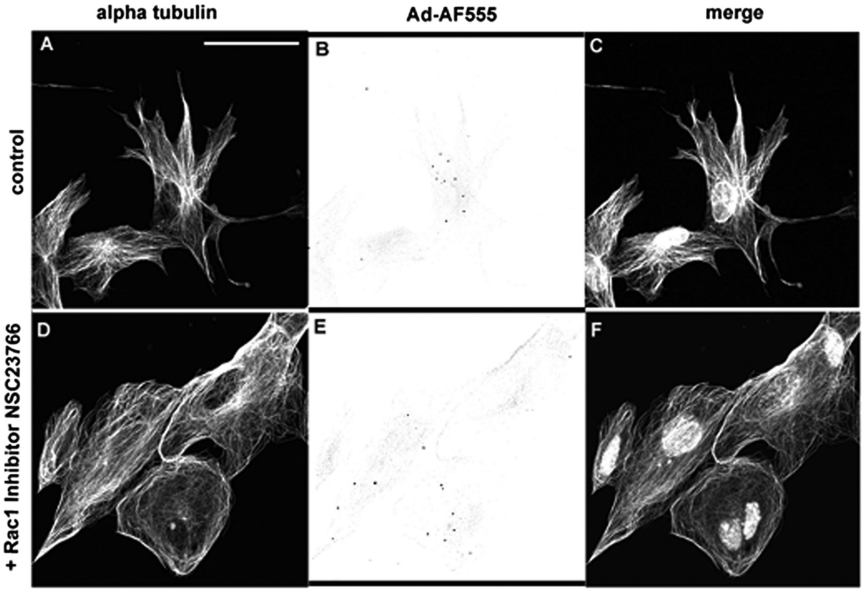

Figure 9. Treatment of HFF cells with 100 μM NSC23766 effectively inhibited Rac1 as demonstrated by the reduction of cellular protrusions in Ad-infected HFF cells. HFF cells infected with Ad-AF555 (10^{10} vp/ml) for 1 h were either untreated (A–C) or pretreated with the Rac1-specific inhibitor NSC23766 (100 μM) for 2 h. Ad was internalized in both untreated (B) and Rac1-inhibited cells (E). Fluorescent labeling of α-tubulin revealed the presence of multiple membrane protrusions in control cells (A), which are not present in Rac1-inhibited cells. The Ad-AF555 images in B and E have been inverted for enhanced clarity, and Ad-AF555 occurs as red spots on the merged images (C and F). Bar, 50 μm.

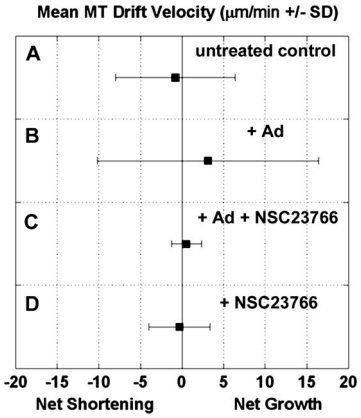

Figure 10. The bias toward MT net growth in Ad-infected cells requires active Rac1. The parameters of dynamic instability were analyzed for MTs in HFF cells, and the mean velocity of MT drift (micrometers per minute ±SD) was calculated for each condition. The broad range of MT drift observed in conditions A and B were expected, because individual MTs experience variable degrees of net growth or shortening during the average imaging time of 56 s. MT drift in uninfected HFF cells (A) was balanced between net growth and shortening, with no bias either way. Ad-infection shifted this balance significantly ($p < 0.05$) toward net growth (B), and this shift involved the presence of pioneer-like MTs which underwent low catastrophe frequency and persistent time in growth compared with uninfected HFF cells. Pretreatment of HFF cells with the Rac1-inhibiting drug NSC23766 (100 μM; 2 h) narrowed the range of MT drift observed in all cells (C and D), so that very few MTs underwent net growth or shortening. In Rac1-inhibited cells, Ad infection did not shift MT dynamics toward net growth (D).

Similar shifts in dynamics have been described for MTs growing into cellular protrusions, termed pioneer MTs. Formation of pioneer MTs requires the activation of the Rho GTPase Rac1 (Wittmann *et al*., 2003). Ad infection activates cellular PI3K (Li *et al*., 1998b) and its downstream effector Rac1 (Greber, 2002), which promote the formation of membrane ruffles and protrusions (Li *et al*., 1998a). To investigate whether the Ad-induced shift in MT dynamic instability requires the activity of Rac1, we treated cells with NSC23766, a drug that has been shown to specifically inhibit the activity of Rac1 in fibroblasts (Gao *et al*., 2004). Untreated HFF cells formed multiple membrane protrusions (Figure 9, A and C). These protrusions were absent from HFF cells treated with NSC23766 (100 μM) for 2 h, indicative of an effective blockage of Rac1-dependent functions (Figure 9, D and F). Ad-associated fluorescence was observed in both NSC23766-treated cells and untreated cells (Figure 9, B and E).

Figure 10 illustrates the differences in MT drift velocity among untreated and Rac1-inhibited HFF cells. As shown above, Ad infection shifted the drift velocity to net growth (Table 2 and Figure 10). Inhibition of Rac1 abrogated this shift in drift velocity so that very few MTs experienced net growth or shortening (Figure 10, Table 2). Rac1 inhibition also prevented the Ad-induced shifts to low MT catastrophe frequency and high MT growth duration (Table 2). These data indicate that Rac1 activity was required for these specific Ad-induced changes to MT dynamics.

DISCUSSION

We found that Ad infection resulted in substantial changes to the host cell MT network. First, Ad infection increased the amount of stable, posttranslationally modified MTs through a RhoA-dependent mechanism. Second, Ad infection modified dynamic instability, shifting the dynamic MTs into an overall state of net growth, through a Rac1-mediated mechanism. The shift to net growth resulted from a decreased MT catastrophe frequency and an increased MT growth time. Third, centrosomal MT nucleation rate increased after Ad infection and MTs regrew at a faster initial rate after nocodazole washout. Overall, our results indicate that the Ad infection process establishes an environment within the host cell that transiently favors the net growth and stability of MTs.

Ad infection caused transient changes to the upstream signaling molecules regulating MT dynamics. Ad-induced RhoA activation peaked at ~15 min and within an hour after infection had recovered close to the level seen in uninfected cells. The timing of RhoA activation after Ad infection is similar to that seen after infection with HHV-8 (Naranatt *et al*., 2005). Furthermore, the timing of these Ad-associated changes in MT dynamics occur within the same time frame as Ad-induced actin rearrangements (Li *et al*., 1998a).

Ad Infection Increases Levels of Posttranslationally Modified MTs

Ad infection increased the amount of both detyrosinated (Glu-MTs) and acetylated MTs in HFF cells. Our results are consistent with studies of other virus systems, including reovirus, HSV1, ASFV, and HHV-8, all of which have been shown to increase the level of acetylated MTs in host cells.

Among these viruses, differences in induced acetylation of MTs include the timing of these changes postinfection, or whether acetylation of MTs occurs as a result of the binding/internalization processes or the viral replication process. Both reovirus- and ASFV-induced acetylation of MTs occurs within the vicinity of viral replication "factories" (Parker *et al*., 2002; Jouvenet *et al*., 2004), suggesting that the acetylation of MTs occurs as a consequence of viral replication. Our observations with Ad infection are more similar to those observed with HHV-8 (Elliott and O'Hare, 1998; Naranatt *et al*., 2005), where acetylation occurs within a few hours of infection. This rapid modulation of MT acetylation is likely a consequence of the virus binding or internalization processes.

It is important to note that MTs need not be stabilized for acetylation of MTs to occur (Palazzo *et al*., 2003). MTs become hyperacetylated after the inhibition of the primary tubulin deacetylase HDAC6 (Hubbert *et al*., 2002). HDAC6 is required for aggresome formation and MT-dependent retrograde transport of misfolded proteins to aggresomes (Kawaguchi *et al*., 2003). HDAC6 also has important roles in some viral infections. The internalization of human immunodeficiency virus (HIV) is regulated by HDAC6, and its overexpression and subsequent deacetylation of MTs inhibited the HIV infection process (Valenzuela-Fernandez *et al*., 2005). ASFV viral replication factories distinctly resemble aggresomes (Heath *et al*., 2001), and as such it is possible that manipulation of HDAC6, not changes in MT stability, leads to the hyperacetylation of MTs after ASFV infection.

Detyrosination of α-tubulin is regulated by RhoA and mDia, acting downstream of FAK and integrin occupancy (Palazzo *et al*., 2004). Detyrosination occurs exclusively on stable MTs, which are capped at their plus ends by a complex which includes +TIPs and mDia (Wen *et al*., 2004). Consistent with these results, we find that Ad infection induces the formation of stable detyrosinated MTs (Glu-MTs) in a RhoA-dependent pathway.

It is not clear whether prolonged activation of RhoA is required to maintain the stability of acetylated or detyrosi-

nated MTs. Our results demonstrate that Ad-infection results in an activation of cellular RhoA within 15 min, returning nearly to baseline by 30–60 min postinfection. A previous study also found that lysophosphatidic acid (LPA)-dependent activation of RhoA is transient, peaking at 3 min and returning to baseline at 30 min after LPA addition (Ren *et al*., 1999). Despite the transience of Ad-induced RhoA activation, we observed posttranslationally modified MTs up to 24 h postinfection (our unpublished data) under continuous infection conditions. LPA-induced Glu MTs were also observed up to 24 h after the initial LPA treatment (Gundersen *et al*., 1994; Nagasaki and Gundersen, 1996). If the RhoA-dependent MT stabilization is due to plus-end capping as described previously (Infante *et al*., 2000), one would expect these capped MTs to remain stable for a prolonged time relative to the initial signal activation.

Ad Infection Increases Centrosomal MT Nucleation

We used EB1-GFP to mark newly polymerized MTs emerging from the centrosome (Piehl *et al*., 2004) and found that Ad infection transiently increased MT nucleation frequency by nearly twofold (Figure 5). This increase in nucleation frequency was consistent with the faster regrowth of MTs from centrosomes observed after removal of nocodazole (Figure 4). We did not observe increased γ-tubulin staining at the centrosomes of infected cells (our unpublished observations), indicating that the increased nucleation rate is not due to a measurable recruitment of this centrosomal protein. As noted previously, the timing of Ad-induced enhancement of MT nucleation frequency does not correspond with Ad accumulation at or near the centrosome.

We have not yet identified whether the Ad-induced enhancement of MT nucleation occurs in a RhoGTPase-mediated manner. Treatment of A549 cells with the Rac1-inhibitor NSC23766 blocked EB1 binding at MT plus ends (our unpublished data). Inhibition of RhoA would also be incompatible with an EB1-based nucleation assay due to EB1 functioning downstream of RhoA (Wen *et al*., 2004).

Two other viruses, vaccinia and ASFV, have been reported to regulate MT assembly from the centrosome, but in these cases virus infection led to decreased MT nucleation and a reduction in γ-tubulin levels at the centrosome (Ploubidou *et al*., 2000; Jouvenet and Wileman, 2005). These viruses replicate at a site near the centrosome, and the disruption of centrosome function is likely a consequence of viral replication (Ploubidou *et al*., 2000; Jouvenet and Wileman, 2005). Contrary to these results, the Ad-induced enhancement of MT nucleation occurred <2 h after infection and was transient.

MT Dynamic Instability Is Regulated by Ad Infection

Ad infection modified MT dynamic instability in both HFF and A549 cells. In each infected cell type, MTs spent more time in growth, underwent catastrophe less frequently, and spent less time in shortening compared with MTs in uninfected cells. Dynamic MTs in infected cells also showed net growth of ~3–5 μm/min, whereas growth and shortening were nearly balanced in uninfected cells. Treatment of HFF cells with a Rac1 inhibitor prevented most of the Ad-induced changes to dynamic instability, but it did not prevent the decreased shortening time observed after viral infection. These results suggest that several MT-associated proteins contribute to the Ad-induced modulation of host cell MT dynamic instability and that only some of these factors are regulated by Rac1.

MTs in Ad-infected cells have dynamic turnover similar to pioneer MTs (Wittmann *et al*., 2003). Pioneer MTs, observed in the extending lamellipodia of PtK cells, are also biased to net growth (~2.4 μm/min), whereas "central" MTs showed balanced growth and shortening (Wittmann *et al*., 2003). Expression of a dominant negative Rac1 blocked formation of pioneer MTs (Wittmann *et al*., 2003). Similarly, our results demonstrate that Rac1 inhibition by NSC23766 blocked the pioneer characteristics of MT growth observed in Ad-infected HFF cells.

Viral Regulation of Host Cell MT Dynamics Should Favor Successful Viral Replication

Ad-infection modifies host cell MT dynamics to a state that should favor viral delivery to the nucleus. After Ad internalization and endosomal escape, efficient MT-mediated translocation to the nucleus is vital for viral replication. Frequent MT catastrophes may be detrimental to the directed MT-mediated transport of cargo within the cell, because even partial depolymerization of the MT at or near the cargo binding site can result in the dissociation of the cargo. In this case, the reassociation of cargo with an existing dynamic MT is limited by diffusion. The free diffusion of particles >50 nm or 500 kDa is inefficient and restricted by molecular crowding and the presence of cytoskeletal barriers (Dohner and Sodeik, 2005). A recent mathematical model of Ad intracellular motility predicted that the rate of Ad vectorial movement within the host cell is inversely proportional to the MT catastrophe rate (Dinh *et al*., 2005). Thus, the ability of viral-induced signals to decrease MT catastrophe frequency could enhance Ad delivery to the nucleus.

Ad-initiated signals could also contribute to viral transport by changing MT dynamics to favor growth. MTs extending toward the cell periphery are more likely to encounter newly internalized virus, making it more likely that the virus and associated dynein motors bind to these MTs. The time required for MTs to find a target, in this case a virus particle, depends on the size of the target, the distance to the target, and the parameters of dynamic instability (Holy and Leibler, 1994). By modifying catastrophe frequency, Ad may enhance "search and capture" efficiency, thereby reducing the time necessary for a MT to come in contact with a relatively small viral target.

Our data provide the first description of virus-induced modulation of the dynamic instability of MTs and further demonstrates the extent to which the host cell cytoskeleton is altered immediately after Ad infection. Previous studies demonstrated that the vimentin network is rapidly reorganization within 5–30 min after Ad infection (Belin and Boulanger, 1987), and changes to the host cell actin cytoskeleton are also well documented (Li *et al*., 1998a). It is now clear that the cytoskeletal rearrangements that occur after Ad-infection include all three cytoskeletal components.

REFERENCES

Aikawa, R., Komuro, I., Yamazaki, T., Zou, Y., Kudoh, S., Zhu, W., Kadowaki, T., and Yazaki, Y. (1999). Rho family small G proteins play critical roles in mechanical stress-induced hypertrophic responses in cardiac myocytes. Circ. Res. *84*, 458–466.

Alblas, J., Ulfman, L., Hordijk, P., and Koenderman, L. (2001). Activation of RhoA and ROCK are essential for detachment of migrating leukocytes. Mol. Biol. Cell. *12*, 2137–2145.

Belin, M. T., and Boulanger, P. (1987). Processing of vimentin occurs during the early stages of adenovirus infection. J. Virol. *61*, 2559–2566.

Bergelson, J. M., Cunningham, J. A., Droguett, G., Kurt-Jones, E. A., Krithivas, A., Hong, J. S., Horwitz, M. S., Crowell, R. L., and Finberg, R. W. (1997). Isolation of a common receptor for Coxsackie B viruses and adenoviruses 2 and 5. Science *275*, 1320–1323.

Desai, A., and Mitchison, T. J. (1997). Microtubule polymerization dynamics. Annu. Rev. Cell Dev. Biol. *13*, 83–117.

Dinh, A. T., Theofanous, T., and Mitragotri, S. (2005). A model for intracellular trafficking of an adenovirus. Biophys. J. *89*, 1574–1588.

Dohner, K., and Sodeik, B. (2005). The role of the cytoskeleton during viral infection. Curr. Top. Microbiol. Immunol. *285*, 67–108.

Elliott, G., and O'Hare, P. (1998). Herpes simplex virus type 1 tegument protein VP22 induces the stabilization and hyperacetylation of microtubules. J. Virol. *72*, 6448–6455.

Gao, Y., Dickerson, J. B., Guo, F., Zheng, J., and Zheng, Y. (2004). Rational design and characterization of a Rac GTPase-specific small molecule inhibitor. Proc. Natl. Acad. Sci. USA *101*, 7618–7623.

Giannakakou, P., Nakano, M., Nicolaou, K. C., O'Brate, A., Yu, J., Blagosklonny, M. V., Greber, U. F., and Fojo, T. (2002). Enhanced microtubule-dependent trafficking and p53 nuclear accumulation by suppression of microtubule dynamics. Proc. Natl. Acad. Sci. USA *99*, 10855–10860.

Glotzer, J. B., Michou, A. I., Baker, A., Saltik, M., and Cotten, M. (2001). Microtubule-independent motility and nuclear targeting of adenoviruses with fluorescently labeled genomes. J. Virol. *75*, 2421–2434.

Graham, F. L., Smiley, J., Russell, W. C., and Nairn, R. (1977). Characteristics of a human cell line transformed by DNA from human adenovirus type 5. J. Gen. Virol. *36*, 59–74.

Greber, U. F. (2002). Signalling in viral entry. Cell Mol. Life Sci. *59*, 608–626.

Gundersen, G. G., Kim, I., and Chapin, C. J. (1994). Induction of stable microtubules in 3T3 fibroblasts by TGF-beta and serum. J. Cell Sci. *107*, 645–659.

Heath, C. M., Windsor, M., and Wileman, T. (2001). Aggresomes resemble sites specialized for virus assembly. J. Cell Biol. *153*, 449–455.

Holy, T., and Leibler, S. (1994). Dynamic instability of microtubules as an efficient way to search in space. Proc. Natl. Acad. Sci. USA *91*, 5682–5685.

Howell, B., Deacon, H., and Cassimeris, L. (1999). Decreasing oncoprotein 18/stathmin levels reduces microtubule catastrophes and increases microtubule polymer in vivo. J. Cell Sci. *112*, 3713–3722.

Hubbert, C., Guardiola, A., Shao, R., Kawaguchi, Y., Ito, A., Nixon, A., Yoshida, M., Wang, X. F., and Yao, T. P. (2002). HDAC6 is a microtubule-associated deacetylase. Nature *417*, 455–458.

Infante, A. S., Stein, M. S., Zhai, Y., Borisy, G. G., and Gundersen, G. G. (2000). Detyrosinated (Glu) microtubules are stabilized by an ATP-sensitive plus-end cap. J. Cell Sci. *113*, 3907–3919.

Jouvenet, N., Monaghan, P., Way, M., and Wileman, T. (2004). Transport of African swine fever virus from assembly sites to the plasma membrane is dependent on microtubules and conventional kinesin. J. Virol. *78*, 7990–8001.

Jouvenet, N., and Wileman, T. (2005). African swine fever virus infection disrupts centrosome assembly and function. J. Gen. Virol. *86*, 589–594.

Kawaguchi, Y., Kovacs, J. J., McLaurin, A., Vance, J. M., Ito, A., and Yao, T. P. (2003). The deacetylase HDAC6 regulates aggresome formation and cell viability in response to misfolded protein stress. Cell *115*, 727–738.

Kelkar, S. A., Pfister, K. K., Crystal, R. G., and Leopold, P. L. (2004). Cytoplasmic dynein mediates adenovirus binding to microtubules. J. Virol. *78*, 10122–10132.

Krishnan, H. H., Sharma-Walia, N., Streblow, D. N., Naranatt, P. P., and Chandran, B. (2006). Focal adhesion kinase is critical for entry of Kaposi's sarcoma-associated herpesvirus into target cells. J. Virol. *80*, 1167–1180.

Leopold, P. L., Ferris, B., Grinberg, I., Worgall, S., Hackett, N. R., and Crystal, R. G. (1998). Fluorescent virions: dynamic tracking of the pathway of adenoviral gene transfer vectors in living cells. Hum. Gene Ther. *9*, 367–378.

Li, E., Stupack, D., Bokoch, G. M., and Nemerow, G. R. (1998a). Adenovirus endocytosis requires actin cytoskeleton reorganization mediated by Rho family GTPases. J. Virol. *72*, 8806–8812.

Li, E., Stupack, D., Klemke, R., Cheresh, D. A., and Nemerow, G. R. (1998b). Adenovirus endocytosis via alpha(v) integrins requires phosphoinositide-3-OH kinase. J. Virol. *72*, 2055–2061.

Maheshwari, G., Jannat, R., McCormick, L., and Hsu, D. (2004). Thermal inactivation of adenovirus type 5. J. Virol. Methods *118*, 141–146.

Matsuyama, A., *et al*. (2002). In vivo destabilization of dynamic microtubules by HDAC6-mediated deacetylation. EMBO J. *21*, 6820–6831.

Meier, O., and Greber, U. F. (2004). Adenovirus endocytosis. J. Gene Med. *6* (suppl 1), S152–S163.

Mittereder, N., March, K. L., and Trapnell, B. C. (1996). Evaluation of the concentration and bioactivity of adenovirus vectors for gene therapy. J. Virol. *70*, 7498–7509.

Nagasaki, T., and Gundersen, G. G. (1996). Depletion of lysophosphatidic acid triggers a loss of oriented detyrosinated microtubules in motile fibroblasts. J. Cell Sci. *109*, 2461–2469.

Naranatt, P. P., Krishnan, H. H., Smith, M. S., and Chandran, B. (2005). Kaposi's sarcoma-associated herpesvirus modulates microtubule dynamics via RhoA-GTP-diaphanous 2 signaling and utilizes the dynein motors to deliver its DNA to the nucleus. J. Virol. *79*, 1191–1206.

Nemerow, G. R., and Stewart, P. L. (1999). Role of alpha(v) integrins in adenovirus cell entry and gene delivery. Microbiol. Mol. Biol. Rev. *63*, 725–734.

Palazzo, A., Ackerman, B., and Gundersen, G. G. (2003). Cell biology: tubulin acetylation and cell motility. Nature *421*, 230.

Palazzo, A. F., Cook, T. A., Alberts, A. S., and Gundersen, G. G. (2001). mDia mediates Rho-regulated formation and orientation of stable microtubules. Nat. Cell Biol. *3*, 723–729.

Palazzo, A. F., Eng, C. H., Schlaepfer, D. D., Marcantonio, E. E., and Gundersen, G. G. (2004). Localized stabilization of microtubules by integrin- and FAK-facilitated Rho signaling. Science *303*, 836–839.

Parker, J. S., Broering, T. J., Kim, J., Higgins, D. E., and Nibert, M. L. (2002). Reovirus core protein mu2 determines the filamentous morphology of viral inclusion bodies by interacting with and stabilizing microtubules. J. Virol. *76*, 4483–4496.

Piehl, M., and Cassimeris, L. (2003). Organization and dynamics of growing microtubule plus ends during early mitosis. Mol. Biol. Cell *14*, 916–925.

Piehl, M., Tulu, U. S., Wadsworth, P., and Cassimeris, L. (2004). Centrosome maturation: measurement of microtubule nucleation throughout the cell cycle by using GFP-tagged EB1. Proc. Natl. Acad. Sci. USA *101*, 1584–1588.

Piperno, G., LeDizet, M., and Chang, X. J. (1987). Microtubules containing acetylated alpha-tubulin in mammalian cells in culture. J. Cell Biol. *104*, 289–302.

Ploubidou, A., Moreau, V., Ashman, K., Reckmann, I., Gonzalez, C., and Way, M. (2000). Vaccinia virus infection disrupts microtubule organization and centrosome function. EMBO J. *19*, 3932–3944.

Ren, X. D., Kiosses, W. B., and Schwartz, M. A. (1999). Regulation of the small GTP-binding protein Rho by cell adhesion and the cytoskeleton. EMBO J. *18*, 578–585.

Rodriguez, O. C., Schaefer, A. W., Mandato, C. A., Forscher, P., Bement, W. M., and Waterman-Storer, C. M. (2003). Conserved microtubule-actin interactions in cell movement and morphogenesis. Nat. Cell Biol. *5*, 599–609.

Rosenfeld, M. A., *et al*. (1992). In vivo transfer of the human cystic fibrosis transmembrane conductance regulator gene to the airway epithelium. Cell *68*, 143–155.

Rusan, N. M., Fagerstrom, C. J., Yvon, A. M., and Wadsworth, P. (2001). Cell cycle-dependent changes in microtubule dynamics in living cells expressing green fluorescent protein-alpha tubulin. Mol. Biol. Cell *12*, 971–980.

Suomalainen, M., Nakano, M. Y., Boucke, K., Keller, S., and Greber, U. F. (2001). Adenovirus-activated PKA and p38/MAPK pathways boost microtubule-mediated nuclear targeting of virus. EMBO J. *20*, 1310–1319.

Valenzuela-Fernandez, A., *et al*. (2005). Histone deacetylase 6 regulates human immunodeficiency virus type 1 infection. Mol. Biol. Cell *16*, 5445–5454.

Vieira, J., and O'Hearn, P. M. (2004). Use of the red fluorescent protein as a marker of Kaposi's sarcoma-associated herpesvirus lytic gene expression. Virology *325*, 225–240.

Vorobjev, I. A., Rodionov, V. I., Maly, I. V., and Borisy, G. G. (1999). Contribution of plus and minus end pathways to microtubule turnover. J. Cell Sci. *112*, 2277–2289.

Webster, D. R., Gundersen, G. G., Bulinski, J. C., and Borisy, G. G. (1987). Differential turnover of tyrosinated and detyrosinated microtubules. Proc. Natl. Acad. Sci. USA *84*, 9040–9044.

Wen, Y., Eng, C. H., Schmoranzer, J., Cabrera-Poch, N., Morris, E. J., Chen, M., Wallar, B. J., Alberts, A. S., and Gundersen, G. G. (2004). EB1 and APC bind to mDia to stabilize microtubules downstream of Rho and promote cell migration. Nat. Cell Biol. *6*, 820–830.

Wickham, T. J., Mathias, P., Cheresh, D. A., and Nemerow, G. R. (1993). Integrins alpha v beta 3 and alpha v beta 5 promote adenovirus internalization but not virus attachment. Cell *73*, 309–319.

Wittmann, T., Bokoch, G. M., and Waterman-Storer, C. M. (2003). Regulation of leading edge microtubule and actin dynamics downstream of Rac1. J. Cell Biol. *161*, 845–851.

Yedowitz, J. C., Kotsakis, A., Schlegel, E. F., and Blaho, J. A. (2005). Nuclear localizations of the herpes simplex virus type 1 tegument proteins VP13/14, vhs, and VP16 precede VP22-dependent microtubule reorganization and VP22 nuclear import. J. Virol. *79*, 4730–4743.